



# Exfoliation of $\beta$ -Ga<sub>2</sub>O<sub>3</sub> Along a Non-Cleavage Plane Using Helium Ion Implantation

Michael E. Liao,<sup>1b</sup>\*,<sup>z</sup> Yekan Wang,<sup>1b</sup> Tingyu Bai, and Mark S. Goorsky

University of California, Los Angeles, Los Angeles, California 90095, USA

An important step in the successful transfer of controlled thickness, wafer-scale  $\beta$ -Ga<sub>2</sub>O<sub>3</sub> layers is demonstrated through exfoliation via helium ion implantation. He<sup>+</sup> ions were implanted into epi-ready (010)  $\beta$ -Ga<sub>2</sub>O<sub>3</sub> substrates at room temperature with an ion energy of 160 keV and a dose of  $5 \times 10^{16}$  cm<sup>-2</sup>. The implanted substrate was then annealed at 200°C followed by 500°C. The lower temperature step initiated He bubble nucleation while the higher temperature step promoted He bubble growth at the projected range beneath the substrate surface. No surface blistering was observed after the 200°C anneal. After the 500°C anneal step, micron-sized surface blistering covering the entire implanted area was observed, confirming exfoliation of  $\beta$ -Ga<sub>2</sub>O<sub>3</sub> along a non-cleavage plane. Triple-axis X-ray diffraction  $\omega$ :2 $\theta$  measurements showed that after annealing at 500°C, the implantation-induced strain was removed. The  $\omega$  scans showed some peak broadening after the low temperature step and more extensive broadening after the high temperature step; this observation corresponds to an increase in lattice plane tilt due to the formation of He bubbles at the projected range. Prior to annealing, scanning transmission electron microscopy images showed a dark contrast at the projected range due to the implantation of a high concentration of He ions. After the 500°C anneal, large cracks at the projected range were observed. These observations match early reports of silicon blistering which, when combined with established direct wafer bonding practices, is expected to lead to large-scale transfer of controlled thickness  $\beta$ -Ga<sub>2</sub>O<sub>3</sub> layers along non-cleavage-plane orientations.  
© 2019 The Electrochemical Society. [DOI: [10.1149/2.0051911jss](https://doi.org/10.1149/2.0051911jss)]

Manuscript submitted September 9, 2019; revised manuscript received October 14, 2019. Published October 24, 2019.

$\beta$ -Ga<sub>2</sub>O<sub>3</sub> is a wide bandgap semiconductor material that is suitable for high-power device applications.<sup>1,2</sup> While  $\beta$ -Ga<sub>2</sub>O<sub>3</sub> has one of the lowest thermal conductivity values compared to other wide bandgap semiconductors, integration with higher thermal conductivity materials can play a key role in implementing  $\beta$ -Ga<sub>2</sub>O<sub>3</sub> in next-generation high-power applications. In the current literature, heterostructures incorporating thin films of  $\beta$ -Ga<sub>2</sub>O<sub>3</sub> grown on various materials such as GaN<sup>3,4</sup> and sapphire<sup>5,6</sup> have already been reported. However, due to the lattice mismatch between dissimilar materials, epitaxy can achieve only a limited number of orientations of  $\beta$ -Ga<sub>2</sub>O<sub>3</sub> depending on the growth substrate.<sup>7,8</sup> Orientation is a crucial parameter to control since many of the properties of  $\beta$ -Ga<sub>2</sub>O<sub>3</sub> are anisotropic due to its low-symmetry monoclinic crystal structure. For example, the [010] direction exhibits the greatest thermal conductivity while along the [100] direction the thermal conductivity is lower by  $\sim 60\%$ .<sup>9</sup> This is especially important for heterojunction structures since the thermal conductivity of a heterojunction interface is dominated by the material with the lowest thermal conductivity.<sup>10</sup> A theoretical study of the electronic properties of  $\beta$ -Ga<sub>2</sub>O<sub>3</sub> showed that the hole effective mass may range from 0.40m<sub>h</sub> to 40m<sub>h</sub> depending on the crystallographic direction, where m<sub>h</sub> is the hole rest mass.<sup>11</sup> Coefficients of thermal expansion (CTE) are pertinent to optimizing processing parameters and even the magnitudes of the CTE along the unit cell axes are not the same, with the a-axis having the lowest value and b-axis the largest.<sup>12</sup> Thus, materials integration via direct wafer bonding will enable a myriad of both orientation and material combinations not realizable through epitaxy.<sup>8</sup> Clearly it is essential to have access to any arbitrary orientation in order to fully utilize the benefits of  $\beta$ -Ga<sub>2</sub>O<sub>3</sub>.

Recent work by Kwon et al.,<sup>13</sup> and Tadjer et al.,<sup>14</sup> have demonstrated a mechanical exfoliation method using tape for obtaining  $\sim 300$  nm to 530 nm thick (100)-oriented, small area  $\beta$ -Ga<sub>2</sub>O<sub>3</sub> layers and transferring the layers to various substrates such as sapphire and diamond. That approach takes advantage of the fact that the (100) plane is one of the two primary cleavage planes<sup>15,16</sup> (the other is (001)) for  $\beta$ -Ga<sub>2</sub>O<sub>3</sub>. Some of the challenges associated with that approach are its incompatibility with large-scale processing and limited crystallographic orientation, i.e. only the (100) and (001) cleavage planes are suitable for this method. Areas of up to only  $\sim 0.4$  mm<sup>2</sup> were successfully transferred to substrates using this mechanical approach.<sup>14</sup> Additionally, Kwon et al.,<sup>13</sup> points out that the thickness of the exfoliated layer from using the tape approach is difficult to control and recycling substrates for subsequent exfoliation becomes more difficult with each

extraction. On the other hand, ion implantation has been shown to exfoliate large wafer-scale areas for many semiconductors.<sup>17,18</sup> When used in conjunction with direct wafer bonding, large areas of thin layers can be transferred to a handle substrate.<sup>18</sup> In addition, thickness is a very well-controlled parameter for exfoliation using ion implantation, and can range from nanometers to microns,<sup>19</sup> depending on the implant energy. Post-exfoliated substrates are also easily recyclable for subsequent exfoliation.<sup>18,20,21</sup>

First introduced to exfoliate layers of silicon, ion implantation of hydrogen<sup>17</sup> or helium<sup>22</sup> and subsequent annealing was used to produce silicon-on-insulator structures. Under the appropriate annealing conditions, an implanted substrate surface will blister from the nucleation and growth of hydrogen or helium gas bubbles present near the implanted species projected range beneath the substrate surface. Surface blistering is an indication of successful exfoliation. If an implanted substrate is bonded to a handle substrate prior to any blister-inducing anneal, uniform wafer splitting can be achieved, resulting in a large-area thin layer transferred to a handle substrate.<sup>17,18</sup> The current literature and previous efforts have further extended the efficacy, analysis, and understanding of hydrogen or helium implantation to silicon,<sup>23-25</sup> germanium,<sup>26</sup> III-V materials,<sup>18,27-29</sup> and II-VI materials<sup>30</sup> where controllable wafer-scale areas of thin layers for various semiconductor materials were successfully exfoliated and transferred. Using ion implantation for thin-film integration naturally fits in the large-scale setting, as outlined by Hayashi et al.:<sup>18</sup> (1) hydrogen or helium ions are implanted in a substrate, (2) the implanted substrate and a handle substrate are direct wafer bonded, and (3) the bonded structure is annealed to promote exfoliation. Regarding  $\beta$ -Ga<sub>2</sub>O<sub>3</sub>, there have been recent reports of direct wafer bonding of 655- $\mu$ m and 680- $\mu$ m thick  $\beta$ -Ga<sub>2</sub>O<sub>3</sub> substrates with SiC by Lin et al.,<sup>10</sup> and Xu et al.,<sup>31</sup> respectively, but there are currently no reports on exfoliating  $\beta$ -Ga<sub>2</sub>O<sub>3</sub> using ion implantation. The ability to exfoliate  $\beta$ -Ga<sub>2</sub>O<sub>3</sub> from non-cleavage plane surfaces, such as (010), makes new device structures possible.

## Experimental

Epi-ready, unintentionally Si-doped (concentration of  $\sim 1 \times 10^{17}$  cm<sup>-3</sup>) Novel Crystal Technology, Inc.<sup>32</sup> (010)  $\beta$ -Ga<sub>2</sub>O<sub>3</sub> substrates were implanted at room temperature with He<sup>+</sup> at an energy of 160 keV and a dose of  $5 \times 10^{16}$  cm<sup>-2</sup>. The implanted substrates were then annealed at 200°C for 12 hours followed by 500°C for up to 6 hours in air on a hot plate. The samples were in direct contact with the hot plate and Al foil was used to cover the samples. This anneal sequence was based on previous work on exfoliation via ion implantation with other semiconductor materials.<sup>18,20,21,25-30</sup> The low temperature step

\*Electrochemical Society Student Member.

<sup>z</sup>E-mail: [meliao@ucla.edu](mailto:meliao@ucla.edu)

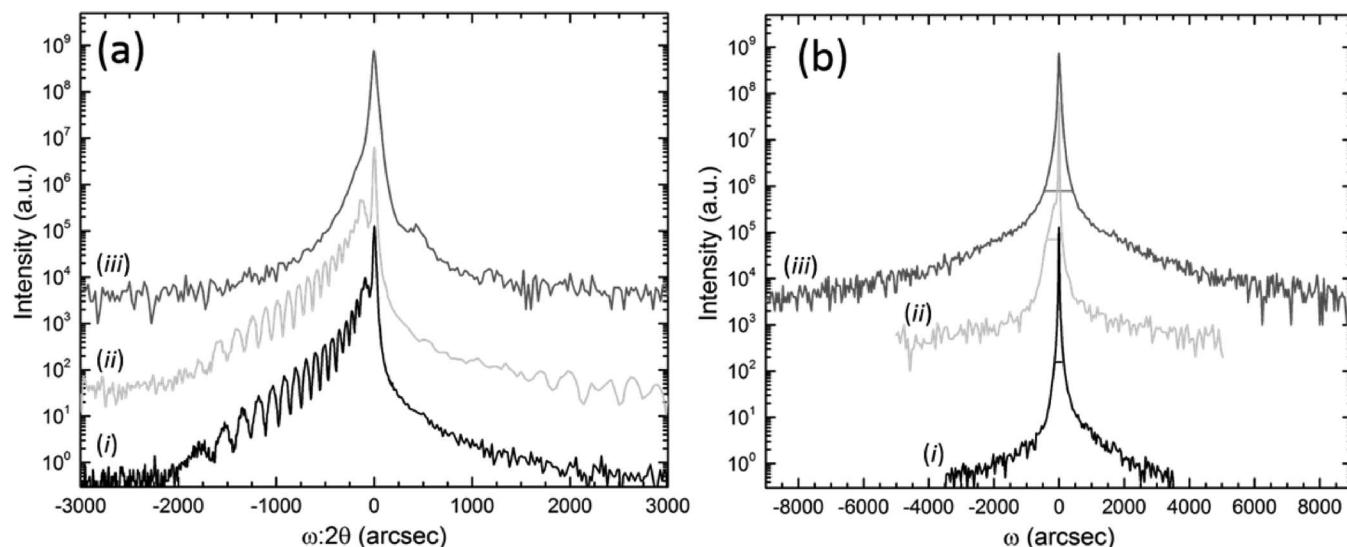


**Figure 1.**  $\omega:2\theta$  (a) and  $\omega$  (b) triple-axis XRD scans of the (020) symmetric reflection for (i) pre-anneal (post-implant), (ii) anneal at 200°C for 12 hours, and (iii) anneal at 200°C for 12 hours followed by 500°C for 6 hours. The horizontal solid bars in (b) mark the FW(0.001)M of each  $\omega$  peak.

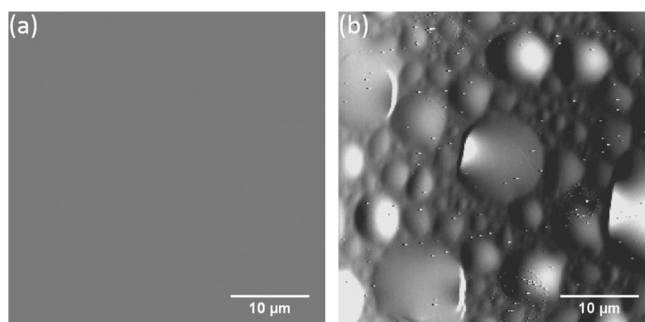
is associated with He blister nucleation which could be correlated to changes in X-ray diffraction (XRD)  $\omega$  curves and the higher temperature step is correlated with growth of the blisters. We attempted individual annealing steps at a series of low temperatures to assess the onset of blister nucleation. After annealing at 200°C for 12 hours, we observed XRD  $\omega$  peak broadening but did not observe blistering at times shorter than 1 hour at 500°C. A high-resolution Bruker-JV D1 diffractometer using triple-axis diffraction<sup>12,33,34</sup> was used to measure  $\omega:2\theta$  and  $\omega$  scans of the (020) symmetric reflection. Both atomic force microscopy (AFM) and Nomarski microscopy images were taken to monitor the surface morphological evolution with annealing. Transmission electron microscopy (TEM) samples were prepared using a FEI Nova 600 DualBeam focused ion beam system. An FEI TITAN S/TEM performed at an accelerating voltage of 300 keV was used to obtain scanning transmission electron microscopy (STEM) images of the implanted region with the samples aligned to the  $[102]$  zone axis. The implantation parameters were used with SRIM<sup>35</sup> to calculate the projected range of the He ions and the displaced atom profile, which were then compared to the STEM measurements.

### Results and Discussion

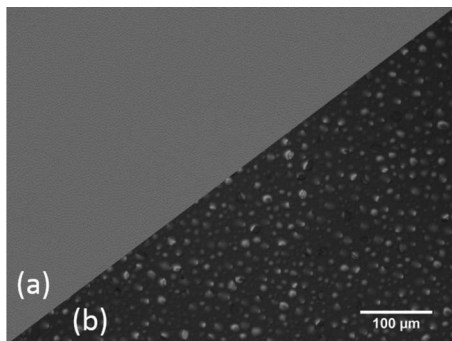
The symmetric (020)  $\omega:2\theta$  line scans and  $\omega$  rocking curves of the pre-annealed (post-implanted) and post-annealed (after the 200°C and 500°C anneal steps) implanted substrate are shown in Figure 1. In this case, the substrate was first annealed at 200°C for 12 hours then subsequently annealed at 500°C for 6 hours. At the pre-anneal stage, oscillations are observed to the left of the main substrate peak in the  $\omega:2\theta$  scan as shown in Figure 1a. These oscillations are associated with tensile strain induced by the implantation caused by the He ions displacing both the Ga and O atoms from lattice sites. This is a common occurrence observed in previous work with implanting other semiconductor materials.<sup>18–21,25–30</sup> The furthest left fringe in the  $\omega:2\theta$  scan typically corresponds to the maximum strain in the implanted region,<sup>19</sup> which is about 1.01%. The strain oscillation intensity decreased and shifted slightly after annealing at 200°C for 12 hours as shown in the  $\omega:2\theta$  scan in plots (i) through (iii) of Figure 1a. This indicates a small amount of diffusion and reconfiguration of the implant-related defects. The  $\omega$  scans for the as-implanted and annealed 200°C samples show full width at half maximum (FWHM) values of 17° in both cases (which is also the same as the non-implanted material). However, the  $\omega$  scan after the 200°C anneal shows peak broadening at the tails of the peak, e.g. the full width at thousandth maximum (FW(0.001)M), from the pre-anneal state (310°) to this annealed state (515°) as shown in

Figure 1b. While FWHM values are more commonly reported, previous work<sup>21,25</sup> demonstrated that the tails of  $\omega$  peaks are more sensitive to changes in crystallinity, i.e. mosaicity or tilt in the exfoliated layer. This tail broadening in the  $\omega$  scan combined with the slight change in the strain profile from the  $\omega:2\theta$  scan is attributed to He gas bubble nucleation at approximately the implant projected range beneath the substrate surface in accordance with earlier work on silicon.<sup>25</sup> After further annealing at 500°C up to 6 hours, the implant-induced strain was fully relieved, as confirmed by the absence of the strain fringes in the  $\omega:2\theta$  scan as shown in Figure 1a. In the corresponding  $\omega$  scan, the FW(0.001)M further broadened to 915° and the FWHM also broadens to 44°. The further broadening of the  $\omega$  peak and loss of the strain is attributed to larger scale defects associated with the implanted He. These results are consistent with exfoliation in other materials in which a lower temperature step (200°C in this study) was used to initiate He bubble nucleation while the higher temperature step (500°C) was used to induce He bubble growth through diffusion.<sup>27</sup>

The surface also showed significant differences before and after the 500°C step and confirms the exfoliation. The surface was then examined with AFM and Nomarski optical measurements as shown in Figures 2 and 3, respectively. 40  $\mu\text{m} \times 40 \mu\text{m}$  AFM scans of the post-implanted  $\beta\text{-Ga}_2\text{O}_3$  surface prior to any annealing showed the same surface morphology and roughness as the pre-implanted surface, which had a surface root mean square (RMS) roughness of  $\sim 0.5$  nm, demonstrating that the as-implanted samples are suitable for subsequent wafer bonding. Figure 2a shows the AFM image of the 200°C



**Figure 2.** AFM scans of the surface after: (a) annealing at 200°C for 12 hours and (b) annealing at 200°C for 12 hours followed by 500°C for 6 hours. Both scans have the same height scale (150 nm).



**Figure 3.** Nomarski images of surfaces (a) annealed at 200°C for 12 hours and (b) annealed at 200°C for 12 hours followed by 500°C for 6 hours.

annealed sample. The roughness remained low ( $\sim 0.8$  nm) after the low temperature annealing step and exhibited the same morphology as the pre-annealed surface. Figure 2b shows significant blistering occurs with the 500°C annealing step (6 hours annealing shown here). On a larger scale ( $600 \mu\text{m} \times 450 \mu\text{m}$  shown here), the Nomarski image in Figure 3a also shows no features on the surface after the 200°C anneal. However, as shown in Figure 3b, a uniform distribution of surface blisters with an  $18 \mu\text{m}$  average diameter is observed over the entire implanted surface with over one third of the surface covered with blisters after the 500°C anneal. Not shown here, it was observed in both Nomarski and AFM images that significant blistering occurred even after one hour at 500°C. The average blister size after annealing at 500°C for one hour was  $1.4 \mu\text{m}$ , which was measured from a  $600 \mu\text{m} \times 450 \mu\text{m}$  Nomarski image. The observed surface blistering and flaking is an indication that exfoliation along the (010) plane for  $\beta\text{-Ga}_2\text{O}_3$  can be readily achieved, which was an important step previously demonstrated with other materials.<sup>17,18</sup> For the case of exfoliation or wafer splitting, the implanted material would need to be bonded to another substrate prior to the high temperature anneal step. In a bonded structure, the bulk of the substrate below the projected range provides the necessary mechanical support to force the energy released during He bubble formation to cause wafer splitting instead of surface blistering.<sup>17</sup>

It can be seen from Figure 3b that some of the blisters completely exfoliated. AFM scans of these exfoliated regions were then measured to examine the exfoliated region morphology as shown in Figure 4. The depth of the two exfoliated blisters shown in Figure 4a were both  $\sim 0.6 \mu\text{m}$ . The results from SRIM<sup>35</sup> simulation calculations are in good agreement with these AFM measurements, which predict the ion projected range to be  $0.64 \mu\text{m}$  with a straggle of  $0.15 \mu\text{m}$  and a displacement per atom peak at a depth of  $0.57 \mu\text{m}$  with a straggle of  $0.21 \mu\text{m}$ . In both of these regions shown in Figures 4b and 4c, distorted rhombus features are observed. However, while there may

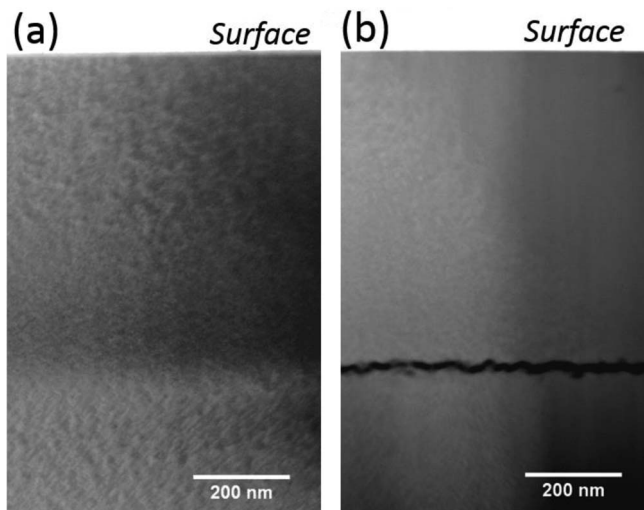


**Figure 5.** HAADF STEM images of the implanted region for (a) post-implant, pre-anneal and (b) post-anneal at 500°C for 1 hour. The sample was aligned to the  $[102]$  zone axis. The measured projected range is approximately  $0.66 \mu\text{m}$ .

be planar relationships for this observed morphology, we have other AFM scans of these exfoliated regions and found that the shapes are somewhat distorted by the AFM measurement itself. Therefore, we do not wish to make a strong claim about the orientational relationships here and plan to assess this issue later. The average minor axis and major axis length for the features shown in Figure 4b are  $91 \text{ nm}$  and  $123 \text{ nm}$ , respectively, while for Figure 4c they are  $85 \text{ nm}$  and  $125 \text{ nm}$ , respectively. The formation of these features at the projected range during the anneal process correspond to the observed widening of the  $\omega$  rocking curves shown in Figure 1b. The exfoliated regions exhibited a  $\sim 4 \text{ nm}$  RMS roughness, which can be smoothed and the features removed with chemical mechanical polishing.

The TEM samples of both the pre-anneal and post-annealed (500°C for 1 hour) implanted substrate were aligned along the  $[102]$  zone axis. The high-angle annular dark-field (HAADF) STEM images are shown in Figure 5. The STEM image of the as-implanted sample shown in Figure 5a shows a dark band parallel to the surface at a depth starting approximately at  $0.6 \mu\text{m}$ . The dark contrast band is  $\sim 0.01 \mu\text{m}$  wide and is likely due to a relatively high He content at the projected range, which was  $\sim 11\%$ . Here, the SRIM<sup>35</sup> simulations are also consistent with the STEM results. After the combined 200°C and 500°C anneal, a relatively uniform crack feature is observed. The height of the crack corresponds to the height of the blister directly above on the surface, which is  $\sim 25 \text{ nm}$  for this particular blister shown in Figure 5b. The

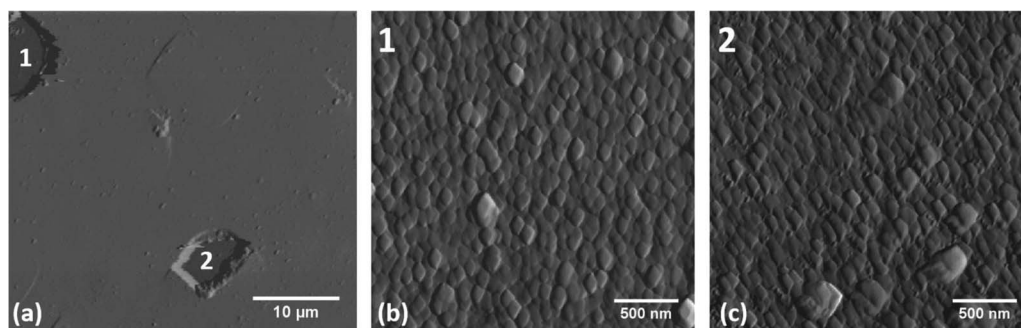


**Figure 4.** A  $40 \mu\text{m} \times 40 \mu\text{m}$  AFM scan after the 500°C for 6 hours step (a) capturing two fully exfoliated blisters (the height scale is  $1 \mu\text{m}$ ). Figures (b) and (c) are  $2.5 \mu\text{m} \times 2.5 \mu\text{m}$  AFM scans of the exfoliated areas in (a), both having the same height scale of  $50 \text{ nm}$ . Note that Figure 2b is similar to Figure 4a but the height scale is much larger for Figure 4a to better show the depth of the craters but the individual blisters are not as readily observed.

average depth of the crack from the surface is 0.66  $\mu\text{m}$ . To obtain other thicknesses using He ion implantation, the He ion implantation energy would be adjusted.

These results can be coupled with the recent studies that have demonstrated that  $\beta\text{-Ga}_2\text{O}_3$  full wafers can be bonded to other substrates. In one study,  $\beta\text{-Ga}_2\text{O}_3$  was bonded to SiC at room temperature and subsequently annealed at 200°C to remove some of the damaged interface.<sup>31</sup> However, there was little further analysis concerning the thermal or electrical properties of the bond. In the other report, good thermal and electrical transport across a bonded  $\beta\text{-Ga}_2\text{O}_3$  full wafer / SiC full wafer interface was achieved after annealing at 1000°C.<sup>10</sup> In both of these cases, the wafers were placed in a vacuum chamber and exposed to an energetic argon beam to facilitate subsequent bonding. Upon bonding, the near surface regions include a damaged layer on each side of the bond that is typically a few nm thick. The wafer pairs that received the argon beam treatment must be annealed at elevated temperatures to remove this damage and to improve the interfacial properties.<sup>36</sup> Our results fit well with the bonding requirements. For example,  $\beta\text{-Ga}_2\text{O}_3$  could be bonded to another wafer using the exposure to an argon beam or simply using a passivation treatment and subsequent annealing.<sup>18,37</sup> The annealing sequence described here would then lead to the transfer of the thin layer (e.g.  $\sim 0.66 \mu\text{m}$  here but that could easily range from 60 nm for 10 keV to 1.2  $\mu\text{m}$  for 400 keV using commercial implanters or even thicker layers using MeV implantation). We note that (at least part of) the 200°C annealing step can be employed prior to the bonding since the surface roughness does not change during this step. After bonding, there can be continued annealing at a low temperature to further improve the bonded interface and potentially remove any interface damage (e.g. from the argon beam treatment<sup>31,36</sup>) and then raised to a high temperature to achieve exfoliation.

### Conclusions

In this study, evidence for  $\beta\text{-Ga}_2\text{O}_3$  exfoliation along the non-cleavage (010) plane using He ion implantation is provided. Surface blistering and flaking were observed after annealing at 200°C for 12 hours followed by 500°C for 1 to 6 hours. The anneal temperatures employed in this study are compatible with current direct wafer bonding procedures of  $\beta\text{-Ga}_2\text{O}_3$  and SiC reported in literature, which use temperatures of 200°C<sup>10</sup> or 1000°C<sup>31</sup> to strengthen the heterojunction bond. The mechanism of exfoliating with ion implantation is applicable to a wide variety of semiconductor materials and works for arbitrary surface orientations.<sup>18–21,25–30</sup> The general mechanism is the nucleation and growth of helium bubbles (or hydrogen as in the literature for other materials) at the projected range beneath the substrate surface to achieve surface blistering or wafer splitting. While this experiment was performed on a (010)-oriented  $\beta\text{-Ga}_2\text{O}_3$  substrate, this process would naturally extend out to other orientations of interest and is expected to lead to materials integration opportunities to take advantage of the desirable properties of  $\beta\text{-Ga}_2\text{O}_3$  (e.g., high field strength) while mitigating some of the less desirable properties (low thermal conductivity).

### Acknowledgments

We appreciate support from the Office of Naval Research through a MURI program, grant No. N00014-18-1-2429.

### ORCID

Michael E. Liao  <https://orcid.org/0000-0003-3103-9357>

Yekan Wang  <https://orcid.org/0000-0001-5959-696X>

### References

- M. A. Mastro, A. Kuramata, J. Calkins, J. Kim, F. Ren, and S. J. Pearton, *ECS J. Solid State Sci. and Tech.*, **6**(5), P356 (2017).
- S. J. Pearton, J. Yang, P. H. Cary IV, F. Ren, J. Kim, M. J. Tadjer, and M. A. Mastro, *Appl. Phys. Rev.*, **5**, 011301 (2018).
- A. Kalra, S. Vura, S. Rathkanthiwar, R. Muralidharan, S. Raghavan, and D. N. Nath, *Appl. Phys. Express*, **11**, 064101 (2018).
- P. Li, H. Shi, K. Chen, D. Guo, W. Cui, Y. Zhi, S. Wang, Z. Wu, Z. Chen, and W. Tang, *J. Mater. Chem. C*, **5**, 10562 (2017).
- S. Ghose, S. Rahman, L. Hong, J. S. Rojas-Ramirez, H. Jin, K. Park, R. Klie, and R. Droopad, *J. Appl. Phys.*, **122**, 095302 (2017).
- V. I. Nikolaev, A. I. Pechnikov, S. I. Stepanov, I. P. Nikitina, A. N. Smirnov, A. V. Chikiryaka, S. S. Sharofidinov, V. E. Bougrov, and A. E. Romanov, *Mat. Sci. Semicond. Processing*, **47**, 16 (2016).
- J. W. Matthews and A. E. Blakeslee, *J. Cryst. Growth*, **27**, 118 (1974).
- Q.-Y. Tong and U. Gösele, *Semiconductor Wafer Bonding: Science and Technology*, (Wiley, New York), p. 8 (1999).
- Z. Guo, A. Verma, X. Wu, F. Sun, A. Hickman, T. Masui, A. Kuramata, M. Higashiwaki, D. Jena, and T. Luo, *Appl. Phys. Lett.*, **106**, 111909 (2015).
- C.-H. Lin, N. Hatta, K. Konishi, S. Watanabe, A. Kuramata, K. Yagi, and M. Higashiwaki, *Appl. Phys. Lett.*, **114**, 032103 (2019).
- J. B. Varley, J. R. Weber, A. Janotti, and C. G. Van de Walle, *Appl. Phys. Lett.*, **97**, 142106 (2018).
- M. E. Liao, C. Li, H. M. Yu, E. Rosker, M. J. Tadjer, K. D. Hobart, and M. S. Goorsky, *APL Mater.*, **7**, 022517 (2019).
- Y. Kwon, G. Lee, S. Oh, J. Kim, S. J. Pearton, and F. Ren, *Appl. Phys. Lett.*, **110**, 131901 (2017).
- M. J. Tadjer, M. A. Mastro, A. Nath, L. E. Luna, T. J. Anderson, K. D. Hobart, and A. Kuramata, *ECS Abstract*, **MA2017-02**, 1233 (2017).
- E. G. Villora, K. Shimamura, Y. Yoshikawa, K. Aoki, and N. Ichinose, *J. Cryst. Growth*, **270**, 420 (2004).
- Z. Galazka, R. Uecker, K. Irmscher, M. Albrecht, D. Klimm, M. Pietsch, M. Brützmam, R. Bertram, S. Ganschow, and R. Fornari, *Cryst. Res. Technol.*, **45**(12), 1229 (2010).
- M. Bruel, B. Aspar, and A.-J. Auberton-Hervé, *Jpn. J. Appl. Phys.*, **36**, 1636 (1997).
- S. Hayashi, M. Goorsky, A. Noori, and D. Bruno, *J. Electrochem. Soc.*, **153**(12), G1011 (2006).
- M. S. Goorsky, ed., *Ion Implantation* (InTech, Croatia), p.65 (2012).
- M. B. Joshi, S. L. Hayashi, and M. S. Goorsky, *Electrochem. Solid-State Lett.*, **11**(8), H236 (2008).
- S. Hayashi, M. B. Joshi, and M. S. Goorsky, *ECS Trans.*, **16**(8), 295 (2008).
- C. Qian and B. Terreault, *J. Appl. Phys.*, **90**, 5152 (2001).
- C. M. Varma, *Appl. Phys. Lett.*, **71**, 3519 (1997).
- X. Lu, S. S. K. Iyer, J. Min, Z. Fan, J. B. Liu, P. K. Chu, C. Hu, and N. W. Chueng, *Proc. 1996 IEEE Int. SOI Conf.*, **96CH35937**, 48 (1996).
- C. Miclaus and M. S. Goorsky, *J. Phys. D: Appl. Phys.*, **36**, A177 (2003).
- I. P. Ferain, K. Y. Byun, C. A. Colinge, S. Brightup, and M. S. Goorsky, *J. Appl. Phys.*, **107**, 054315 (2010).
- S. Hayashi, D. Bruno, and M. S. Goorsky, *Appl. Phys. Lett.*, **85**, 236 (2004).
- S. Hayashi, R. Sandhu, and M. S. Goorsky, *J. Electrochem. Soc.*, **154**(4), H293 (2007).
- E. Padilla, M. Jackson, and M. S. Goorsky, *ECS Trans.*, **33**(4), 263 (2010).
- C. Miclaus, G. Malouf, S. M. Johnson, and M. S. Goorsky, *J. Electron. Mater.*, **34**(6), 859 (2005).
- Y. Xu, F. Mu, Y. Wang, D. Chen, X. Ou, and T. Suga, *Ceramics International*, **45**, 6552 (2019).
- Novel Crystal Technology, Inc., <https://www.novelcrystal.co.jp/eng/>
- B. Poust, B. Heying, S. Hayashi, R. Ho, K. Matney, R. Sandhu, M. Wojtowicz, and M. Goorsky, *J. Phys. D: Appl. Phys.*, **38**, A93 (2005).
- M. Liao, C. Campbell, C.-Y. Tsai, Y.-H. Zhang, and M. Goorsky, *J. Electron. Mater.*, **47**(10), 5666 (2018).
- J. F. Ziegler, J. P. Biersack, and U. Littmark, *The Stopping and Range of Ions in Solids* vol 1 (Oxford, Pergamon), (1985).
- M. E. Liao, C. Li, C. Flötgen, and M. S. Goorsky, *ECS Trans.*, **86**(5), 55 (2018).
- M. J. Jackson, B. L. Jackson, and M. S. Goorsky, *J. Appl. Phys.*, **110**, 104903 (2011).